 doi:10.20944/preprints202209.0059.v1

Mechanical, thermal, and chemical properties of PLA-Mg filaments produced via colloidal route for Fused Filament Fabrication

Jaime Orellana-Barrasa[a]*, Ana Ferrández-Montero[b], Aldo. R. Boccaccini[c], Begoña Ferrari[b], José Ygnacio Pastor[a]

[a] *Centro de Investigación en Materiales Estructurales (CIME), Universidad Politécnica de Madrid, 28040 Madrid, Spain*
[b] *Instituto de Cerámica y Vidrio (CSIC), Campus de Cantoblanco, 28049 Madrid, Spain*
[c] *Institute of Biomaterials, Department of Materials Science and Engineering, University of Erlangen-Nuremberg, Cauerstrasse 6, 91058 Erlangen, Germany*

*Corresponding author: jy.pastor@upm.es

Abstract

The effect of Mg particles on PLA's thermal, chemical, physical, and mechanical properties has been studied. The thermal and physical properties have been studied by differential scanning calorimetry, analysing the stability of the α and α'-crystals of the PLA. A colloidal route was used to introduce Mg particles inside the PLA matrix, ensuring a good dispersion of the particles. Materials with Mg contents from 0 to 10 wt.% have been prepared, with additions of polyethyleneimine (PEI) and polyethylene glycol (PEG). Fourier Transform Infrared Spectroscopy has been used to confirm the influence of Mg, PEI, and PEG on PLA properties. The mechanical properties have been measured with a universal tensile test machine on printed filaments via Fused Filament Fabrication (FFF), which were naturally aged to stable conditions. Filaments with and without a notch were studied to obtain the materials' tensile strength, elastic modulus, and fracture toughness. Different analytical models to explain the results of the PLA-Mg were studied, in which the interface strength of the PLA-Mg composites was calculated.

Keywords PLA-Mg, FTIR, DSC, crystallinity, tensile test

1. Introduction

PLA-Mg composite materials are promising biodegradable biomaterials for improving the healing process of bone tissues. The repair of damaged bone is still a significant concern nowadays. This has led to a large amount of research on topics like bone grafts [1], bone cement [2], [3], scaffolds [4], [5], hydrogels [6], or cell treatments [7], to try to regenerate bone when the damage produced is considerable large compared with its healing capacity. Adding growth factors or other chemicals, like calcium phosphates or Mg, can enhance the regenerative properties of biomaterial strategies.

Mg is an essential component of the human body. Since 1935, it has been used as a biomaterial [8]. One of its roles is to support the formation of bone tissue by promoting both the proliferation and differentiation of stem cells into osteoblasts; Mg has osteogenic properties [9], [10]. Because of this, Mg can be used to promote the healing or recovery of damaged bone tissue in patients with any bone defect, like traumas, tumours, or inflammations, that need the formation of new bone. However, introducing Mg directly into the body can produce issues related to the release and local accumulation of hydrogen, a degradation product of Mg, which is a highly corrodible metal [10], [11].

 doi:10.20944/preprints202209.0059.v1

Moreover, for the optimum healing conditions of bone tissue, it has been found that controlling the degradation rate of the implant is essential, as the implant will also provide mechanical support [12]. One option for exploiting the osteo-promotive benefits of Mg while controlling its fast degradation rate is by creating a composite in which the Mg particles are dispersed in a bioabsorbable material that slowly releases the Mg. For this purpose, PLA is an excellent material, as it is biocompatible, and its degradation rate inside the human body can be tuned.

PLA is also a common material used in additive manufacturing, specifically in filament fused fabrication (FFF) processes. In this thermal extrusion process, the PLA-matrix is melted, extruded in specific locations, and then cooled down. This process can also be done with the PLA-Mg composite, and implants or scaffolds can be produced that perfectly match the damaged bone. This strategy of using PLA as a matrix and then printing structures has been previously explored by loading the PLA with other organic and inorganic materials like chitosan [13], bioactive glass [14], graphene [15], carbon nanotubes [16], cellulose [17], or hydroxyapatite [18]. Several methods are described in the literature for adding Mg particles into a polymer matrix [19]. This work has studied the influence of the Mg particle addition on the PLA's thermal, chemical, physical and mechanical properties when it is added through the colloidal route developed by Ferrández-Montero et al. in earlier works [1]–[4].

Our previous study gained knowledge on how the thermal extrusion process affects the PLA [20].It was found that the PLA, after being printed, had lower thermal and mechanical properties, which slowly increased with natural ageing until they stabilised at values more associated with PLA. In this research, we aim to understand the effect of Mg introduced through the colloidal route in PLA after the extrusion process via FFF, as this is the method for producing PLA-Mg scaffolds of interest for bone regeneration applications. This will provide a more profound knowledge of the basic science, supporting this promising material for improving the healing process of bone tissues.

Differential Scanning Calorimetry was used to figure out the impact of Mg addition on the thermal and physical properties of PLA. This technique can find exothermal and endothermal reactions in the material, which can be correlated with the described responses of PLA in the literature, like its crystallisation of the α or α' form [21]. This polymorphism of PLA is essential for its properties, as it is related to its mechanical properties, barrier properties, thermal properties, and degradability properties, among others [22]. Together with the Fourier Transform Infrared Spectroscopy (FTIR) spectrum of PLA, which is well described in the literature[23], [24], it is possible to obtain different results about the effect of Mg on PLA. FTIR is an extremely sensitive technique for detecting any variation in chemical bonds [25]. These chemical bonds affect the configuration and packing of the macromolecules, thus making it an excellent technique for analysing crystallinity changes of the PLA [26]. Archimedes tests have been used to calculate the density and porosity of the material, which are highly related to mechanical properties. Tensile tests on filaments with a notch can provide information on the fracture toughness of the materials, which ultimately controls the tensile strength of PLA. Knowing the density, porosity, composition, and fracture toughness, it has been possible to calculate the theoretical tensile strength for each material, which has been later compared with the measured values of the tensile strength providing important information about these materials, like the interface strength between the PLA matrix and the dispersed Mg particles.

This paper introduces new results on how Mg particles affect the properties of PLA, complementing our previous studies on PLA, in which the natural ageing of printed filaments and the evolution of their properties with natural ageing were investigated [20].

Preprints (www.preprints.org) | NOT PEER-REVIEWED | Posted: 5 September 2022 doi:10.20944/preprints202209.0059.v1

2. Materials and methods

2.1 Production of the material

PLA filaments, 1.75 mm in diameter, were produced by melting and extruding the PLA pellets supplied by NatureWorks (Ingeo biopolymer 2003D, a high molecular weight PLA with M_w 182.000 g/mol and a 4.25% content in d-lactide [20]). A colloidal route was observed for the 1.75 mm PLA-Mg filaments[27], [28]. The PLA is first dissolved in tetrahydrofuran (THF, from Panreac, Germany) in this colloidal route. Mg particles are covered with polyethyleneimine (PEI with M_w 25.000 g/mol from Sigma Aldrich, Germany). Briefly, PEI-Mg modified particles were mixed in suspension with PLA and polyethylene glycol (PEG 400 from Sigma Aldrich, a low molecular weight plasticiser with 400 g/mol). The suspension was dried and granulated under vacuum, and granules were extruded in 1.75 mm filaments with 2.5, 5.0, 7.5 and 10 wt.% of Mg. A scheme of the material is shown in figure 1.

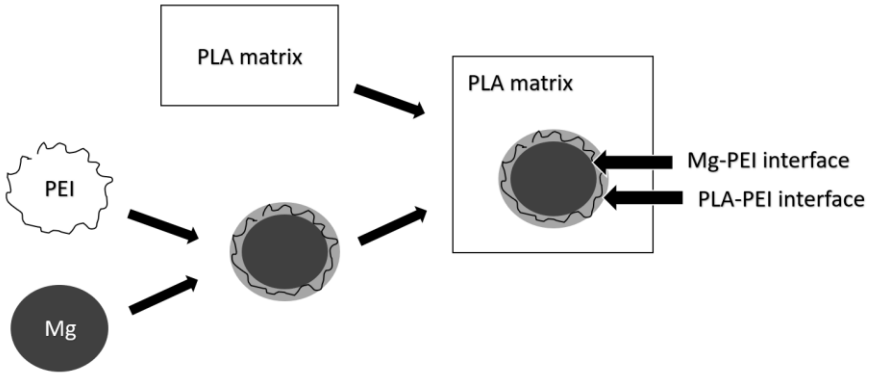

Figure 1 – Scheme of the PLA-Mg composite processing, making explicit the PEI interface between the PLA matrix and the Mg particles. On the materials with Mg, PEG was added to the PLA matrix to improve printability.

PLA and PLA-Mg filaments were thermally extruded via FFF at 190 ºC and 155 ºC, respectively, in ambient humidity and room temperature conditions. The addition of PEG makes the printability of PLA-Mg filaments possible at 155 ºC. Filaments with 300 to 400 microns in diameter were obtained. A PRUSA i3 MK3S with a 0.4 mm nozzle was used.

Considering our previous study on PLA [20], at least three months are necessary for the complete natural ageing of PLA without Mg particles. Thus, all samples have been naturally aged inside zip-bags with desiccant and protected from solar light radiation for a minimum of 90 days before testing.

2.2 Differential scanning calorimetry

Differential scanning calorimetry was performed with a Mettler Toledo 822e instrument inside a 40 µL aluminium crucible, at a heating rate of 10 ºC/min from 40 to 210 ºC, on 5-10 mg of material (the printed filament) cut down in pieces of 2-4 mm length. All the materials were carefully placed inside Al crucibles, ensuring that all pieces were in contact with the bottom of the crucible. This was important as it has been found through this research that slight shifts (± 1 ºC) in the temperature peaks can be produced if the configuration of the filaments inside the crucible changes. The material PLA-7.5Mg was evaluated at different heating rates: 1, 3, 10 and 20 ºC/min. For the calibration of the DSC device, an Indium standard was used.

Preprints (www.preprints.org) | NOT PEER-REVIEWED | Posted: 5 September 2022 doi:10.20944/preprints202209.0059.v1

2.3 Fourier Transform Infrared Spectroscopy

Fourier Transform Infrared Spectroscopy (FTIR) has been done with a IRAffinity-1S from SHIMADZU. The samples were analysed from 200 scans in the mid-IR (400 to 4000 cm^{-1}) in absorbance, apodisation with the Happ-Genzel function, and a resolution of 1 cm^{-1}

2.4. Archimedes' test

Archimedes' tests were performed inside ethanol in a Mettler Toledo Balance coupled to an LC-Density device, following the same procedure as in our previous study [20]. It has been found that more consistent and accurate results were obtained using ethanol instead of distilled water due to the better wettability between PLA and ethanol, avoiding the formation of tiny bubbles around the filaments.

The theoretical density values for each composition were calculated using the rule of mixtures. The difference between the experimental results and the calculated theoretical ones was used to figure out each composition's porosity. For the calculations of the theoretical densities, the following values were used: 1.240 g/cm^3 for the PLA, 1.125 g/cm^3 for the PEG, and 1.738 g/cm^3 for the Mg.

2.5 Tensile tests, notch and fractographies

All samples were tested following the same method for the tensile tests described in our previous study [20], following the UNE-EN ISO 527-1:2019 standard: samples of 20 mm were tested at 1 mm/min with a 1 kN load cell in an INSTRON 5866, glued to cardboard to avoid inducing mechanical damage from the clamps, with rotulas to prevent stresses due to rotations or bends, and aged a minimum of 90 days at room temperature inside zip bags with desiccant. A scheme of the tensile test is shown in figure 2.

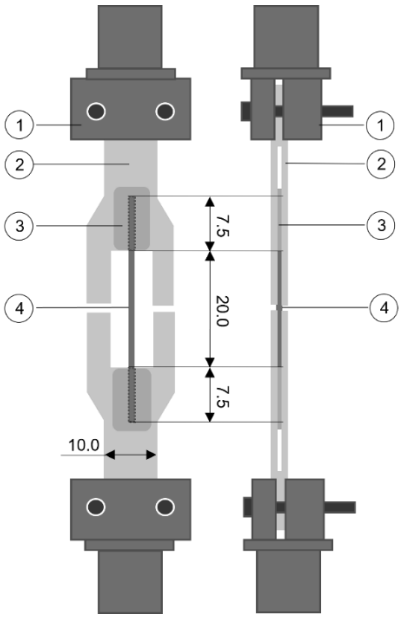

Figure 2 – Tensile test scheme: 1) mechanical clamp, 2) cardboard, 3) cyanoacrylate-based adhesive as a chemical clamp, 4) PLA or PLA-Mg filament. Units in millimetres.

The fracture toughness (K_{IC}) was measured on the filaments by making a notch perpendicular to its longitudinal direction with the help of a sharp blade (coherent with the indications of the European Structural and Integrity Society (ESIS)) and a carved plate of steel. Although each sample was

 doi:10.20944/preprints202209.0059.v1

carefully analysed before and after the fracture, the notch depths were approximately half the filament diameter. A NIKON PROFILOMETER with a resolution of 1 µm was used to measure the dimensions of the notches. Tensile tests were performed on filaments with notches under the same conditions described before, and the fracture toughness was calculated using the James and Mills equation [27] based on research group experience.

Details of fracture surfaces were taken with an AURIGA FESEM ZEISS, prior to deposition of a 20 nm thickness carbon coating with a LEIKA carbon metalliser.

2.6 Modelling

Rule of mixtures was used for modelling the elastic modulus, considering the elastic modulus of Mg and PLA as 45 GPa [28] and 3.6 GPa [20], respectively. The modelled materials were considered homogeneous and isotropic. Interface strength between PLA matrix and Mg particles was calculated by the best fitting to the experimental data, assuming the interfaces between PLA-PEI-Mg as only one, referred to as PLA-Mg interface.

For modelling the tensile strength on PLA-Mg composites, it was considered: 1) the interface strength previously calculated and 2) the fracture toughness experimentally measured for each PLA-Mg composition. Further details are provided through the discussion.

3. Results and discussion

3.1 Mg/PLA filaments s characterisation

Regarding the results obtained from the DSC at 10 ^{o}C/min, there are significant differences in the thermal properties with adding Mg particles, as shown in figure 3. All the reactions analysed are indicated in that figure: glass transition, enthalpic relaxation, crystallisation of α' and α forms, melting of α' and α forms. Table 3 summarised different values extracted from the DSC graphs.

Preprints (www.preprints.org) | NOT PEER-REVIEWED | Posted: 5 September 2022 doi:10.20944/preprints202209.0059.v1

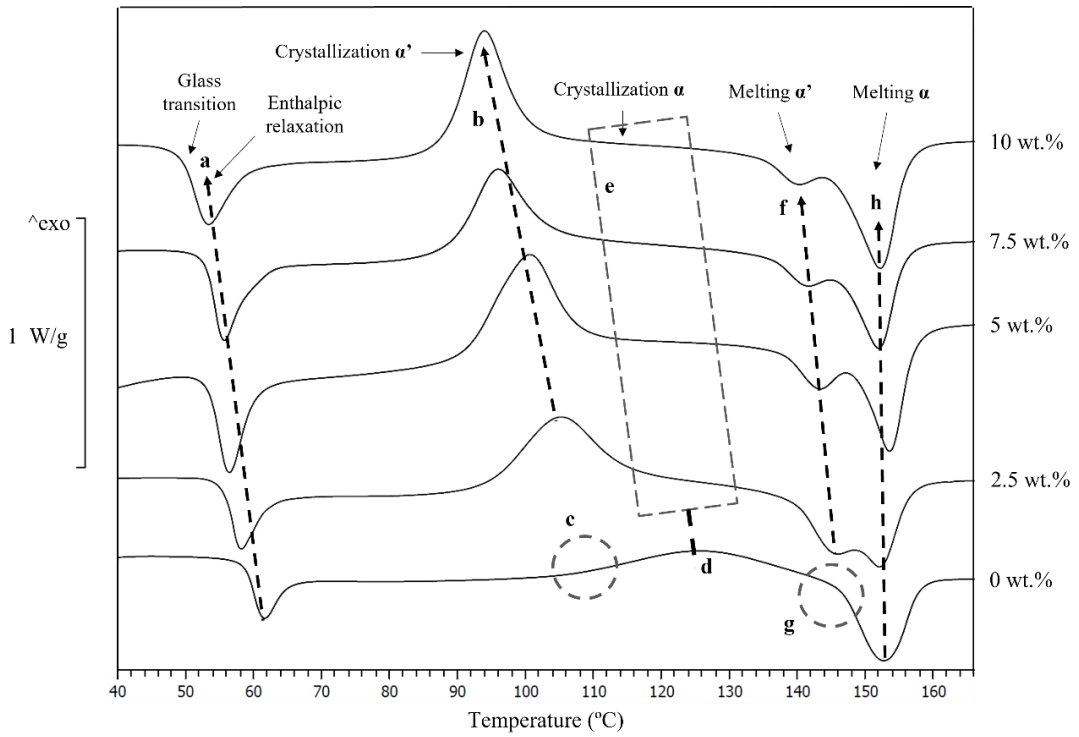

Figure 3 – DSC at 10 °C/min of PLA and PLA-Mg with 0, 2.5, 5, 7.5 and 10 Mg. a) Evolution of glass transition and enthalpic relaxation toward lower temperatures, b) apparition of α' crystallisation', shifting towards lower temperatures with the increase of Mg content, c) missing α' crystallisation 'in neat PLA d) well-defined α crystallisation and on PLA without Mg, e) uncertain shape of α crystallisation on PLA-Mg composites, f) of melting α' appeared in samples with Mg, g) missing α' melting ' in PLA without Mg.

Table 3. Thermal properties of extruded 1D PLA and PLA-Mg filaments at a scanning rate of 10 °C/min. T_g: glass transition; T_{ER}: enthalpic relaxation temperature; ΔH_{ER}: enthalpy of enthalpic relaxation; $T_{cc.\alpha'}$ and $T_{cc.\alpha}$: cold crystallisation temperature of α' and α crystals, respectively; $T_{m.\alpha'}$ and $T_{m.\alpha}$: melting temperature of α' and α crystals, respectively. Following IUPAC's convention, positive enthalpy changes indicate that the material absorbs the energy, which indicates an endothermal reaction. Melting and crystallisation enthalpies have not been included in the table, as providing an accurate value was tricky due to the overlap of the reactions.

%Mg	Heating rate (°C/min)	T_g (°C)	T_{ER} (°C)	ΔH_{ER} (J/g)	$T_{cc.\alpha'}$ (°C)	$T_{cc.\alpha}$ (°C)	$T_{m.\alpha'}$ (°C)	$T_{m.\alpha}$ (°C)
0	10	59.9 ± 0.5	62.6 ± 0.5	4.5 ± 0.1	-	125 ± 1	-	151 ± 1
2.5	10	54.9 ± 0.5	58.0 ± 0.5	5.1 ± 0.1	105 ± 1	-	146 ± 1	152 ± 1
5.0	10	52.3 ± 0.5	56.4 ± 0.5	8.6 ± 0.2	100 ± 1	-	143 ± 1	153 ± 1
7.5	10	49.8 ± 0.5	53.3 ± 0.5	7.0 ± 0.2	96 ± 1	-	142 ± 1	152 ± 1
10	10	48.7 ± 0.5	53.3 ± 0.5	8.1 ± 0.2	94 ± 1	-	140 ± 1	152 ± 1

PLA's **glass transition** was decreased with the addition of Mg particles. This property is related to enthalpic relaxation; consequently, the **enthalpic relaxation temperature** also decreases. The evolution of these two properties with the addition of Mg particles is shown in figure 4. The evolution of both properties fits well with a quadratic equation, stabilising to a value with the higher percentages of Mg in the material.

Preprints (www.preprints.org) | NOT PEER-REVIEWED | Posted: 5 September 2022 doi:10.20944/preprints202209.0059.v1

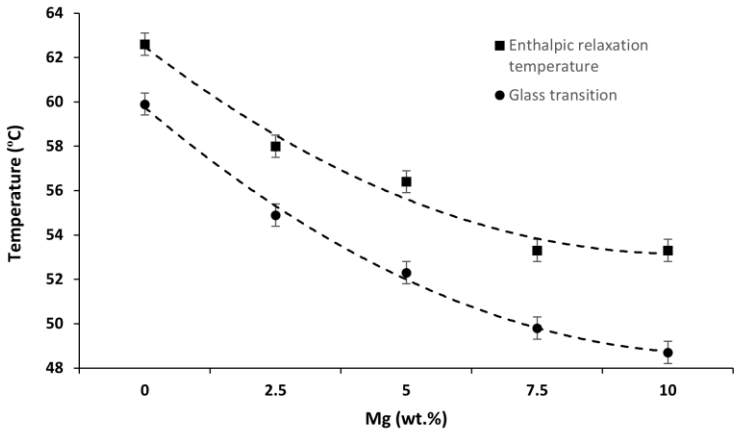

Figure 4 - Glass transition and enthalpic relaxation temperatures of PLA and PLA-Mg composites. Experimental results in bold, dashed lines for the quadratic approximation.

Another observation from DSC values in table 3 is the higher **enthalpic relaxation enthalpy** on PLA-Mg composites compared with neat PLA. In our earlier study [20], the enthalpic relaxation enthalpy of the same PLA increased up to 366 days, and no signs of reaching a stable value were observed after one year of natural ageing. As PLA-Mg composites are running higher values for the enthalpic relaxation enthalpy after similar ageing times, writes down faster natural ageing of the PLA-Mg composites compared with the neat PLA. Cangialosi et al. [29] described faster ageing due to the addition of silica nanoparticles, explaining this acceleration with the tendency of nanoparticles to occupy the free volume of the polymer, being the free volume nanoscale voids of space due to an inefficient packing of polymers [30]. However, it was described that this acceleration was faster with the smaller the particle. Our Mg is not in the scale of nanometres but micrometres (30 microns average particle diameter). To explain this faster natural ageing of the PLA-Mg, we must address other phenomena discussed later.

A shift towards lower temperatures of the crystallisation reactions with the increase of Mg was observed. By visually comparing the areas in figure 2, higher crystallisation enthalpies were also noticed on PLA-Mg composites compared with neat PLA. Note that this does not provide information on the crystallinity forms at room temperature. Closely looking at the DSC graphs, it was observed that the new crystallisation peaks that appeared with the addition of Mg start at temperatures around 80 to 90 ^{o}C and end at 115 to 120 ^{o}C. This temperature range corresponds with the beginning and end of the α' crystallisation [21] . This α' crystallisation was not observed in neat PLA samples. The reaction indicated as α' crystallisation in figure 2 has a shoulder to the right side. This is coherent with the existence of an α crystallisation reaction in that area, like the one observed on neat PLA. However, due to the overlap of α and α' crystallisation reactions, it is difficult to assess any conclusion on the α crystallisation with the DSC. Because of all this, it is concluded that a considerable increment in the α' crystallisation reaction has appeared in all the PLA-Mg materials, and that it occurs at lower temperatures with adding more Mg. To explain the decrease in the α' crystallisation temperature, we need to address the Mg role as a catalyser for the crystallisation of the PLA. The higher the percentage of Mg, the more nucleation points and the earlier will be observed the α' crystallisation. With this, it is suggested that **Mg particles could function as stabilisers of the α' form.**

Moreover, in figure 3, it is seen that appears a new endothermal reaction at temperatures between 140 to 146 ^{o}C after the **melting response** from the PLA without Mg. This new peak in the PLA-Mg

 doi:10.20944/preprints202209.0059.v1

materials is coherent with the melting of α'-crystals previously formed [21]. The melting peak at 151 - 153 ^{o}C in figure 3, which stays constant with adding Mg, corresponds to the melting of the α-crystals.

The changes in the thermal properties described up to this point (decrease of T_g, an increase of natural ageing rate, a decrease of α' crystallinity temperature, and growth of α' crystallisation enthalpies) could be explained by a decrease in the molecular weight of the PLA matrix in the PLA-Mg during the colloidal processing. The literature describes a decrease of the molecular weight by depolymerisation with the addition of Mg particles [31]; however, FTIR results have shown no significant changes in the peaks related to the -OH terminal groups [32]. In fact, the molecular weight decrease depends on the printing conditions [33].

The second hypothesis relates to the plasticiser PEG added to the PLA-matrix on the PLA-Mg composites. The literature describes the effect of plasticiser triphenyl phosphate (TPP) on PLA crystallisation reaction, which shifts the reaction to lower temperatures and increases its crystallisation rate [34]. It is coherent with the literature that the PEG as a plasticiser facilitates the crystallisation reaction, as well as decreasing the glass transition and accelerating the natural ageing of PLA.

The combination of all the previous hypotheses is the most probable explanation for the results previously described: 1) the crystallinity induced by Mg particles, 2) the decrease of PLA-matrix molecular weight with the addition of Mg particles, and 3) the addition of PEG. '''Regarding the third reason, the weight percentage of PEG in the PLA remains constant for all PLA-Mg materials. Thus, a decrease of the molecular weight by depolymerising the PLA-matrix with the addition of Mg particles [31] could explain the decrease of T_g with increasing Mg particles in the composite.

It was studied the PLA-7.5Mg at different heating rates on the DSC to further understand the α'-crystal stabilisation by the Mg. Results are shown in figure 4. In Table 4 are summarised the calculated values from the DSC graphs.

Preprints (www.preprints.org) | NOT PEER-REVIEWED | Posted: 5 September 2022 doi:10.20944/preprints202209.0059.v1

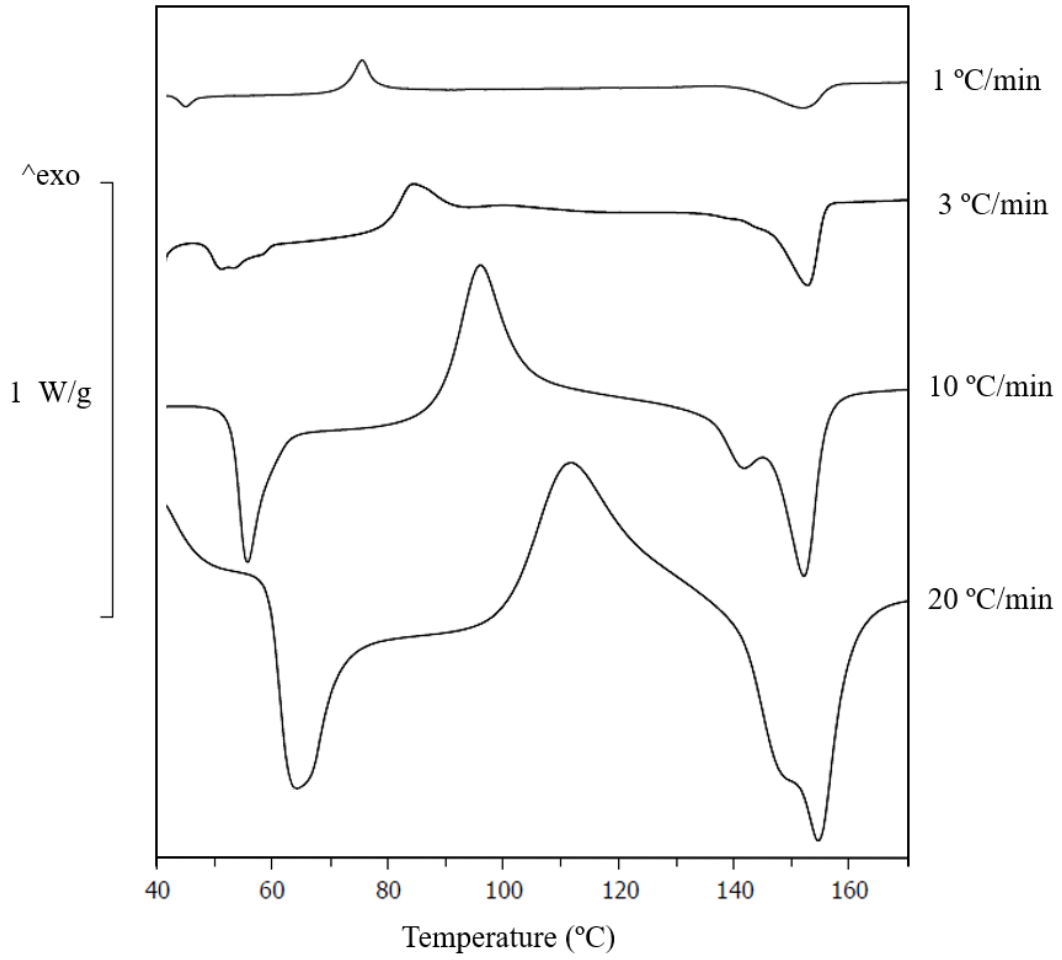

Figure 5 – DSC of PLA-7.5Mg at different heating rates from 1 to 20 °C/min. Scale bar for material heated at 10 °C/min.

Table 4. Thermal properties of the extruded 1D PLA and PLA-Mg filaments. T_g: glass transition; T_{ER}: enthalpic relaxation temperature; ΔH_{ER}: enthalpy of enthalpic relaxation; $T_{CC.\alpha'}$ and $T_{CC.\alpha}$: cold crystallisation temperature of α' and α crystals, respectively; $T_{m.\alpha'}$ and $T_{m.\alpha}$: : melting temperature of $\boldsymbol{\alpha}'$ and $\boldsymbol{\alpha}$ crystals, respectively. Following IUPAC's convention, positive enthalpy changes say that the material absorbs the energy, which indicates an endothermal reaction.

%Mg	Heating rate (°C/min)	T_g (°C)	T_{ER} (°C)	ΔH_{ER} (J/g)	$T_{CC.\alpha'}$ (°C)	$T_{CC.\alpha}$ (°C)	$T_{m.\alpha'}$ (°C)	$T_{m.\alpha}$ (°C)
7.5	1	42.8 ± 0.5	45.0 ± 0.5	2.4 ± 0.1	76 ± 1	-	-	152 ± 1
7.5	3	48.2 ± 0.5	50.7 ± 0.5	4.6 ± 0.1	84 ± 1	100 ± 1	-	153 ± 1
7.5	10	49.8 ± 0.5	53.3 ± 0.5	7.0 ± 0.2	96 ± 1	-	142 ± 1	152 ± 1
7.5	20	59.8 ± 0.5	64.2 ± 0.5	8.5 ± 0.2	112 ± 1	-	147 ± 1	154 ± 1

The α'conversion into α crystals is a thermally driven process in which time is essential. This process involves the dynamics of the PLA macromolecules, and thus, faster heating rates should not give enough time for the conversion of the α' into α crystals. Changing the scanning rates makes it possible to differentiate which reactions are happening inside the PLA.

Looking the scan at 1 °C/min, in figure 5, it is only observed that the α' crystallisation and the peak associated with the melting of α'-crystals was reduced to the left shoulder on the melting of the α-crystals. This indicates a conversion of α' into α during the DSC scan, what would be expected if our previous hypothesis for the new peaks related to the α' in the PLA-Mg composites' are correct. Looking at increasing heating rates (1, 3, 10 and 20 °C/min) in figure 5, the melting enthalpies of α'-

Preprints (www.preprints.org) | NOT PEER-REVIEWED | Posted: 5 September 2022 doi:10.20944/preprints202209.0059.v1

crystal rise, indicating a higher melting of α' crystals and that the reaction of α' conversion into α has not had enough time to be completed.

Looking in detail the graph at 3 °C/min, in figure 6, there are observed two reactions:

The first one is a decoupling in the α' and α crystallisation reactions, figure 6.a, which provides a precise α crystallisation temperature for a PLA-7.5Mg material, which could not be defined before for any PLA-Mg composite. Notice that the temperature peaks depend on the scanning rate by comparing the α' crystallisation temperatures in figure 4. The α crystallisation temperatures were 100 ºC for the PLA-7.5Mg and 115 ºC for the PLA. As a direct comparison with the results in figure 2 is not possible, a DSC of neat PLA at 3 ºC/min was done. It was concluded that the α crystallisation also happens at lower temperatures on the PLA-7.5Mg compared with the neat PLA, which could not be told before.

The second one is figure 6.b, an exothermal reaction in the left shoulder of the α melting shoulder that corresponds to the melting of α'. This exothermal peak is related to the energy released during the transformation of α' into α [35]–[37], which can extend up to temperatures around 150 °C, at heating rates of 2 °C/min [21]. This is coherent with the literature and, as previously discussed for the crystallisation enthalpies, the overlap of reactions is a challenge for making a precise analysis of the PLA melting enthalpies, as several reactions overlap at the same time: the conversion of α' into α and the melting of α' and α.

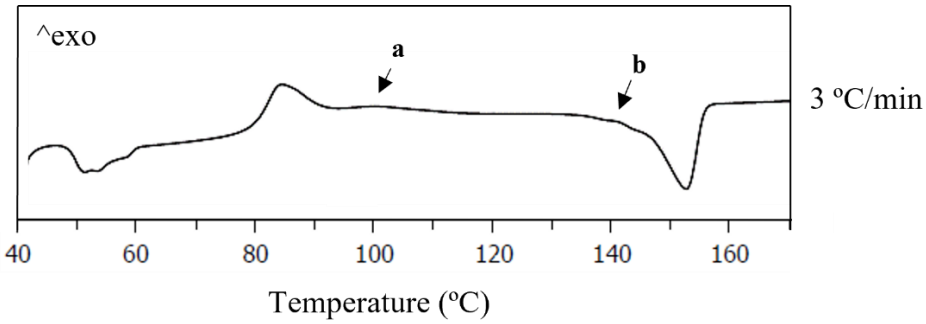

Figure 6 – Detail of PLA-7.5Mg at 3 °C/min. a) α crystallisation, b) transformation of α' into α at the same time α' is melting.

FTIR was performed to further understand PLA and PLA-Mg composites produced through the colloidal process to analyse bonds related to the α' and α crystals, interactions between PEG and PLA; the interaction between PEI and PLA.

FTIR results are shown in figure 7. Slight variations between PLA and PLA-Mg composites were observed, saying that the chemical bonds present in PLA and PLA-Mg composites were similar at room temperature, coherent with the literature [38].

Preprints (www.preprints.org) | NOT PEER-REVIEWED | Posted: 5 September 2022 doi:10.20944/preprints202209.0059.v1

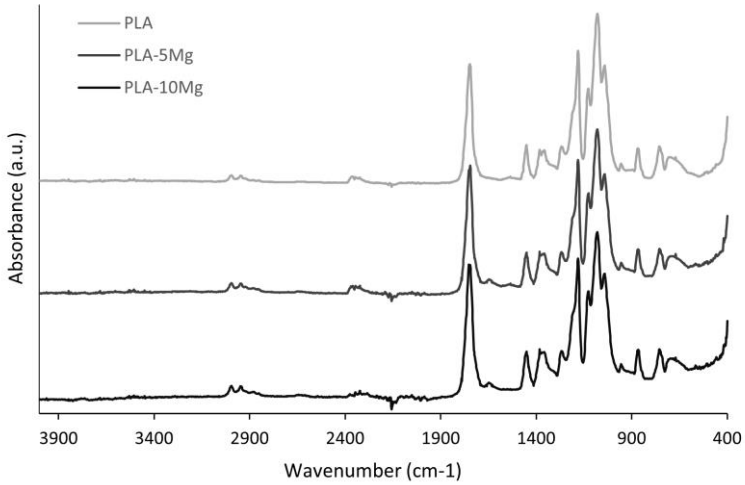

Figure 7 – FTIR spectrum of PLA, PLA-5Mg and PLA-10Mg.

Regarding the results on α' and α crystal structures in PLA and PLA-Mg composites at room temperature, small shifts were found at peaks related to PLA's crystallinity. Rodrigues et al. [39] described a shift in the peak at 1748 cm^{-1}. Ferrández et al. [32] analysed this peak on PLA-Mg tap and other peaks at 867 cm^{-1}, 1266 cm^{-1}, and 1382 cm^{-1}, bands related to the polymorphism of PLA, specifically with α and α' crystals. Our results on these peaks, represented in figure 8, were:

Peaks related to α-crystals:

- At 867 cm^{-1}, shift from 868 cm^{-1} to 866 cm^{-1} on PLA with Mg particles.
- At 1748 cm^{-1}, split into two peaks at 1754 cm^{-1} and 1746 cm^{-1} on PLA with Mg particles.

Peaks related to α'- crystals:

- At 1266 cm^{-1}, remains stable.
- At 1382 cm^{-1}, remains stable.

These results are interesting as it is obtained that α-crystals are affected by adding Mg during the cooling of the PLA-Mg. However, the PLA studied here has a high d-lactide percentage (4.25%), and percentages above 2% are expected to produce neglectable crystallinity percentages during the cooling regarding the literature, explaining the minor variation on the FTIR peaks related at room temperature with the α' and α in figure 7.

Preprints (www.preprints.org) | NOT PEER-REVIEWED | Posted: 5 September 2022 doi:10.20944/preprints202209.0059.v1

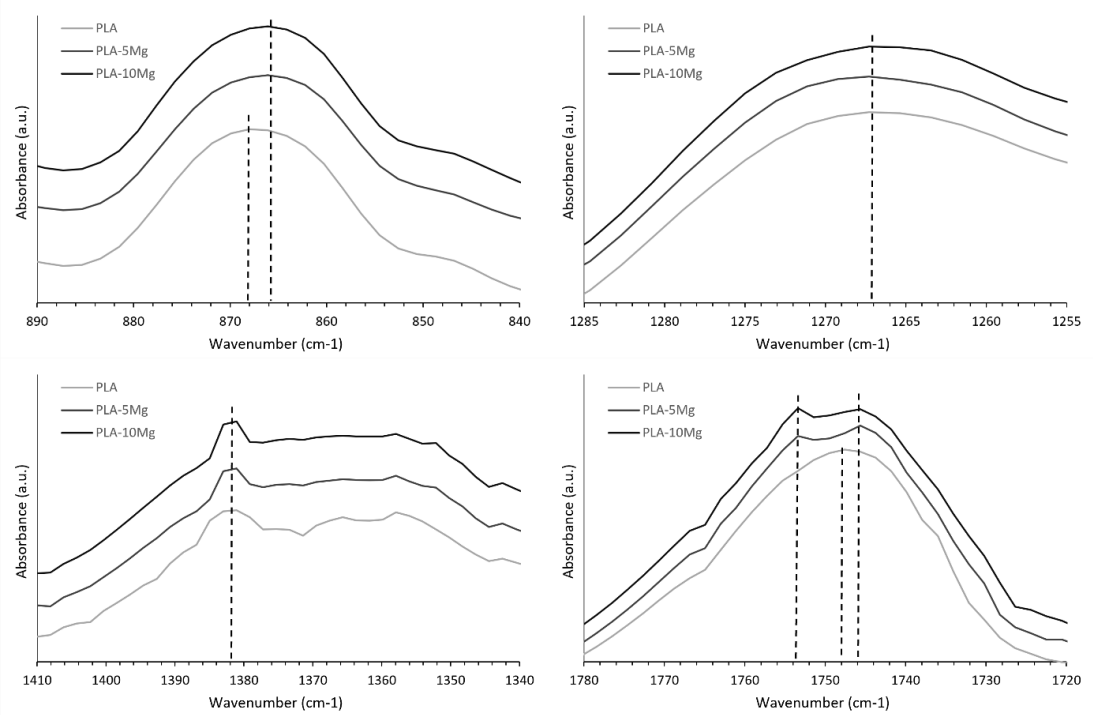

Figure 8 – FTIR detail of **α** and **α'** forms peaks on PLA and PLA-Mg composites. From left to right, top to bottom, detail of peak at: 867 cm^{-1}, 1266 cm^{-1}, 1382 cm^{-1}, and 1748 cm^{-1}.

Regarding the PEG interaction with the PLA matrix and Mg particles, no significant changes are associated with PEG peaks, coherent with [40].

As stated before, PEI was added to improve the stability of the Mg during the colloidal processing. In the FTIR a peak was observed at 1647 cm^{-1}. This is not present in neat PLA (0 wt.% Mg), as shown in figure 9. A decrease in the 2850 cm-1 is observed with the increase of Mg particles on the sample and, consequently, with the increase of PEI. This decrease is associated with the reaction of PLA ester groups with -NH on the PEI. This provides support to the interaction between PLA and PEI.

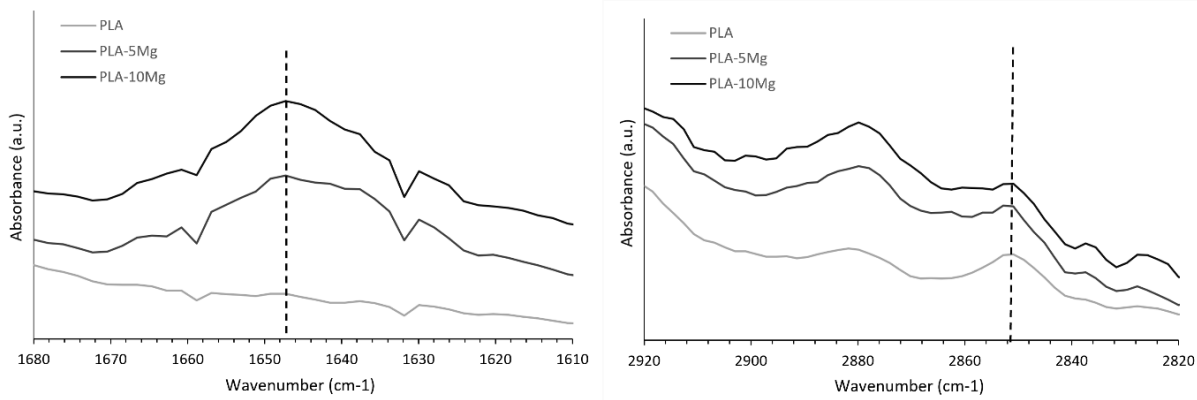

Figure 9 – FTIR details related to PEI on PLA and PLA-Mg composites.

The Archimedes' test provided information about the density of PLA and PLA-Mg composites. Results are shown in figure 10.

Preprints (www.preprints.org) | NOT PEER-REVIEWED | Posted: 5 September 2022 doi:10.20944/preprints202209.0059.v1

The density slightly increases up to 1 % with adding Mg particles. However, this increase is below the expected theoretical value. This discrepancy was related to the rise of porosity inside the material, confirmed with SEM images. The closed porosity for each composition was calculated using the difference between density experimental and theoretical values.

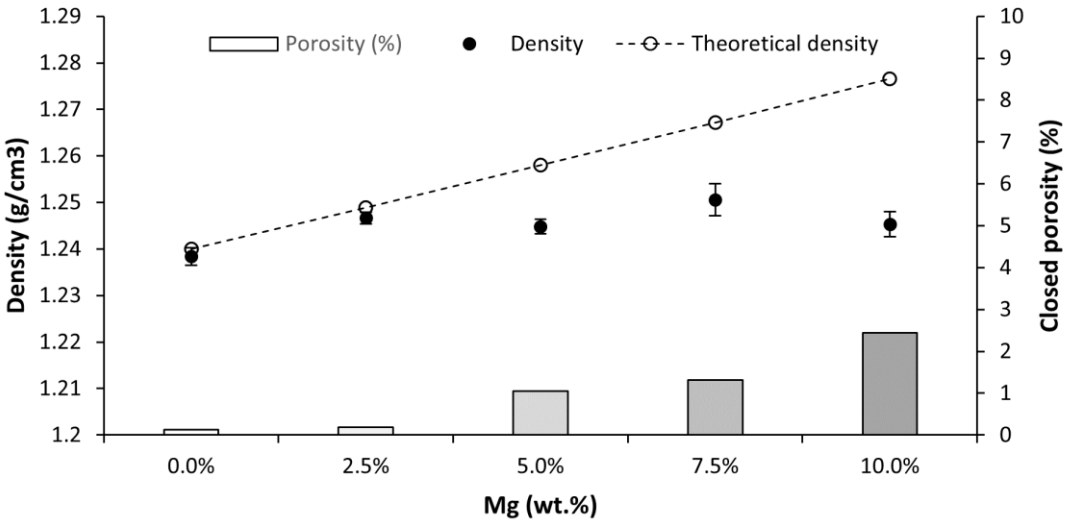

Figure 10 – Density and closed porosity compared with the weight percentage of Mg content in the PLA and PLA-Mg composites.

3.2 Mechanical tests and fractography

Due to the higher elastic modulus of the Mg, it was expected to increase the elastic modulus from the theoretical point of view. However, a slight decrease in the elastic modulus with adding **Mg** was obtained from the experimental tests.

Comparing the experimental elastic modulus with the theoretical ones for each PLA-Mg composite, figure 4 shows that the Mg is providing none of its mechanical properties to the matrix, indicating a weak interface between **the PLA and the Mg.**

It is essential to clarify that the weak interface is not between the PLA and the Mg, as the interface is PLA-PEI-Mg. The model has considered the PLA-PEI-Mg interface as only one interface, but as shown in figure 1, there are two interfaces: the PLA-PEI and the Mg-PEI. With our model, one of these interfaces is demonstrated to be weak, as the Mg is not providing its mechanical properties to the composite. This concludes that at least one of the interfaces, PLA-PEI or PEI-Mg, is not strong enough to carry mechanical loads. To determine which of the two interfaces is the weak one, we need to refer to the chemistry of the formed bonds. Because the adhesion between the PEI and the PLA is excellent, based on covalent bonds, and there is evidence of it on the FTIR, it can be determined that the weak interface is between PEI and Mg. However, even though the chemical bonding between the PEI and the Mg is not strong enough to transmit significant mechanical loadings, it can avoid the aggregation of Mg particles during colloidal processing.

Figure 11 also shows the influence of previously calculated porosity on the elastic modulus. The effect is neglectable compared with the bond strength between the PLA and the Mg.

Preprints (www.preprints.org) | NOT PEER-REVIEWED | Posted: 5 September 2022 doi:10.20944/preprints202209.0059.v1

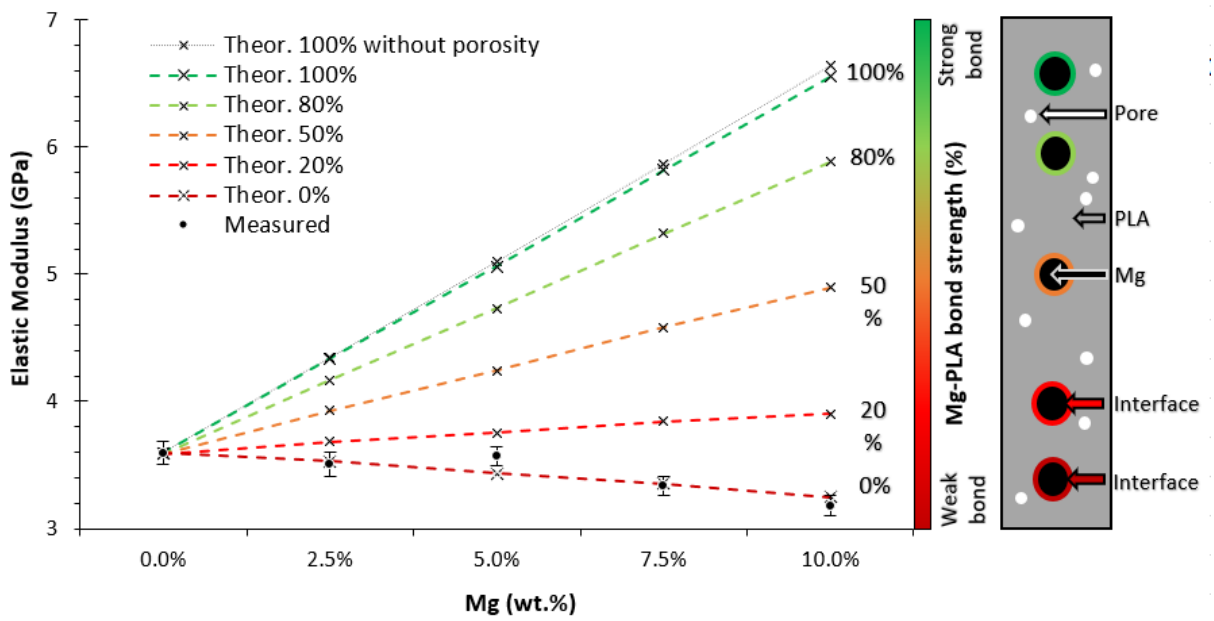

Figure 11 – Elastic modulus versus the Mg content and its theoretical value considering the porosity and the PLA-Mg bond strength. Bond strength of 100% states for a perfect interface in which all loads are transmitted to the Mg particle; 0% states for a weak interface where loads are not transferred from the PLA-matrix to the Mg particle.

Regarding SEM images of the fracture surfaces after the tensile tests, figure 12 shows that the size of the Mg particles is on the expected values regarding the Mg particle volumetric distribution [26] and how the Mg particles are detached from the PLA matrix on the fracture surfaces after the tensile tests. This last result further supports a relatively weak PLA-PEI-Mg interface from a mechanical point of view, even though it is excellent from the chemical point of view since, regarding the FTIR, there is evidence of the PLA-PEI bond on the printed materials. The PEI-Mg is the weakest bond in the interface, and due to the stresses induced during the tensile test, the Mg particles were detached. PEI-Mg is the most fragile bond in the PLA-PEI-Mg interface, and it can be broken due to the stresses produced during the tensile tests, as these results have not been observed before on samples broken by a thermal shock using liquid nitrogen [32].

In figure 12, it was also observed that Mg particles are well dispersed and that no agglomerates were created in none of the samples studied under the SEM, a significant advantage of manufacturing PLA-Mg composites through the colloidal process.

Preprints (www.preprints.org) | NOT PEER-REVIEWED | Posted: 5 September 2022 doi:10.20944/preprints202209.0059.v1

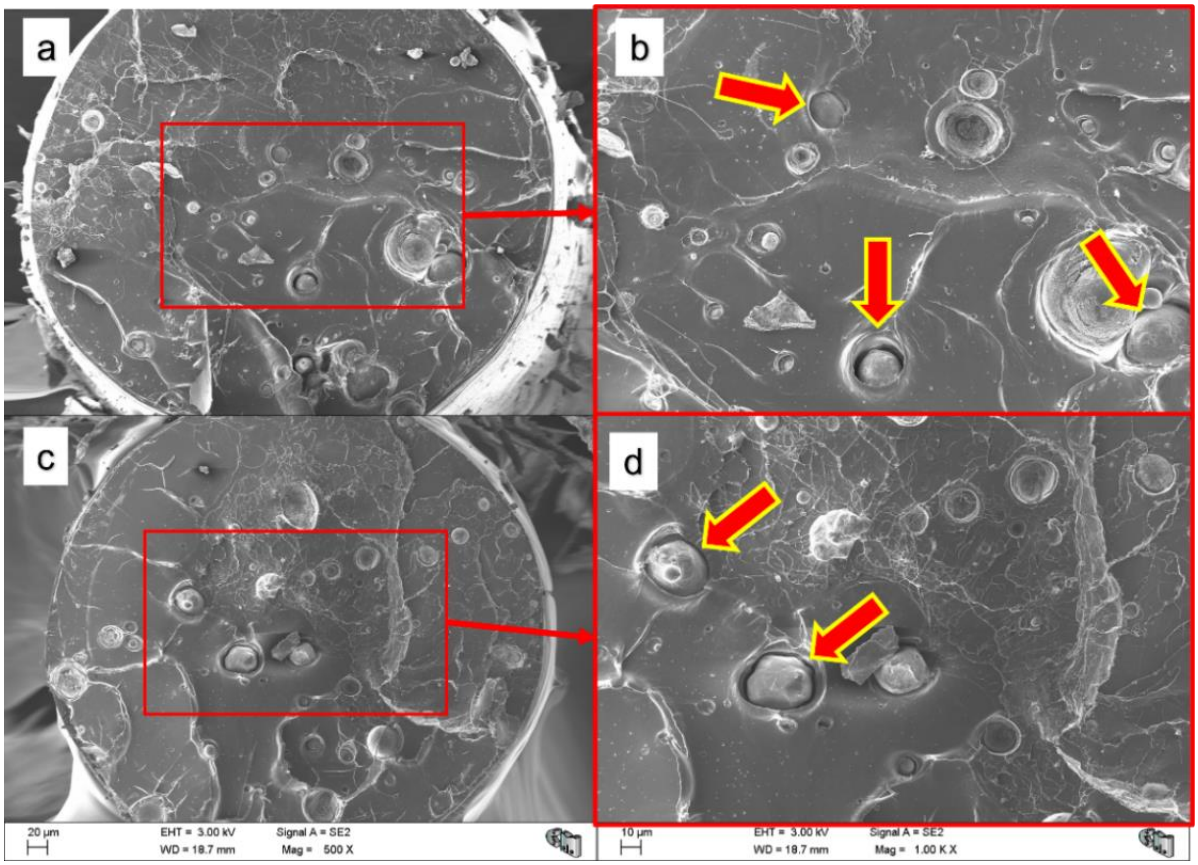

Figure 12 – SEM fractographies of PLA-5Mg after tensile tests at 1 mm/min. Arrows indicate the Mg particles detached from the PLA-matrix after a tensile test.

Once the elastic modulus was understood, and the bond strength between PLA and Mg particles was not strong enough (due to the PEI-Mg bond) to transmit significant mechanical forces, **tensile strength** and **fracture toughness** were studied. These two properties are highly interrelated, as tensile strength depends on both the fracture toughness and the defects in the material, equation 1,

$$K_{IC} = \sigma \Upsilon \sqrt{\pi a_c} \quad (1)$$

where K_{IC} is the fracture toughness, σ is the stress, Υ is a geometrical factor and a_c is the crack length. Note that the more significant the crack length or the size of the defect, the lower the required stress for breaking the material, known as the tensile strength.

The tensile strength was calculated using the same tensile tests to obtain the elastic modulus. Nevertheless, figure 13 a) and b) filaments with a notch were tested for fracture toughness. The notch tip radius was 1 µm, as shown in figure 13 c). Figure 13 d) to f) provide details of the notched fibres. Interestingly, in 13 f) an Mg particle was split by the blade. The Mg particle is observed to be well attached to the PLA-matrix; however, this is just the size in which the blade has produced compression during the notching. On the size in which tensile stresses pulled out the matrix due to the cutting movement of the blade, it is observed that the PLA matrix was utterly separated from the Mg particle.

Preprints (www.preprints.org) | NOT PEER-REVIEWED | Posted: 5 September 2022 doi:10.20944/preprints202209.0059.v1

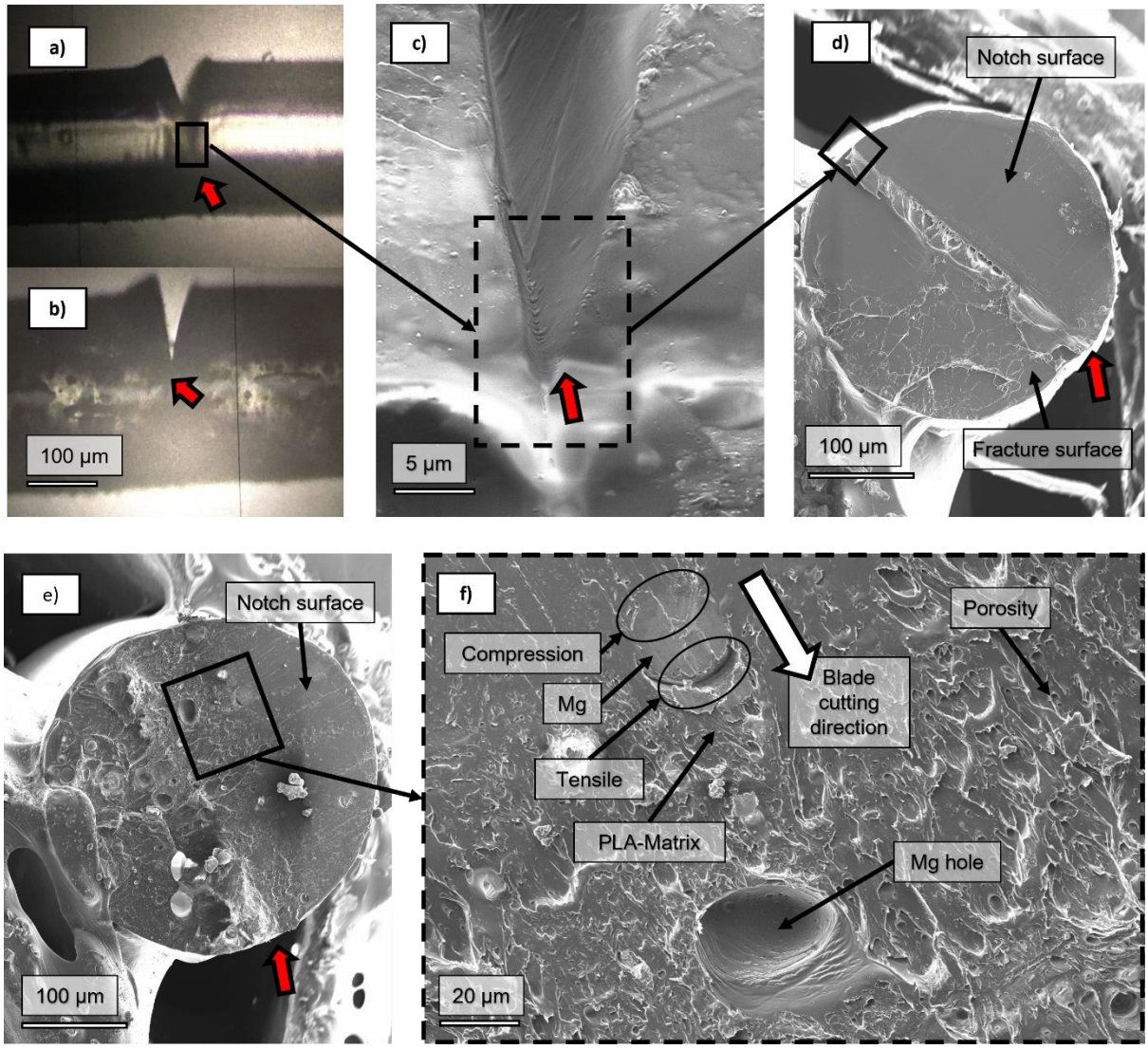

Figure 13 – Detail of the notch performed on PLA and PLA-Mg samples and fracture surface: a) PLA filament with notch; b) PLA-Mg filament with notch; c) Detail of the notch from a lateral view, and notch tip radius of 1 µm; d-e) Notch and crack surface after tensile test of PLA and PLA-5Mg respectively; f) Detail of PLA-5Mg notch surface. Small arrows indicate the edge of the notch.

The experimental results of the fracture toughness are shown in figure 14. Looking at the PLA-Mg composites, **it is observed that increasing the content in Mg reduces fracture toughness**. If extrapolated to neat PLA (0% Mg), this trend indicates that neat PLA should have a higher fracture toughness, and indeed, it does. Comparing neat PLA with PLA-2.5Mg, a considerable decrease in fracture toughness can be observed. It can be confirmed that the PLA- Mg composites are more brittle than the neat PLA. It can also be established that **the higher the amount of Mg particles, the lower the fracture toughness**.

Preprints (www.preprints.org) | NOT PEER-REVIEWED | Posted: 5 September 2022 doi:10.20944/preprints202209.0059.v1

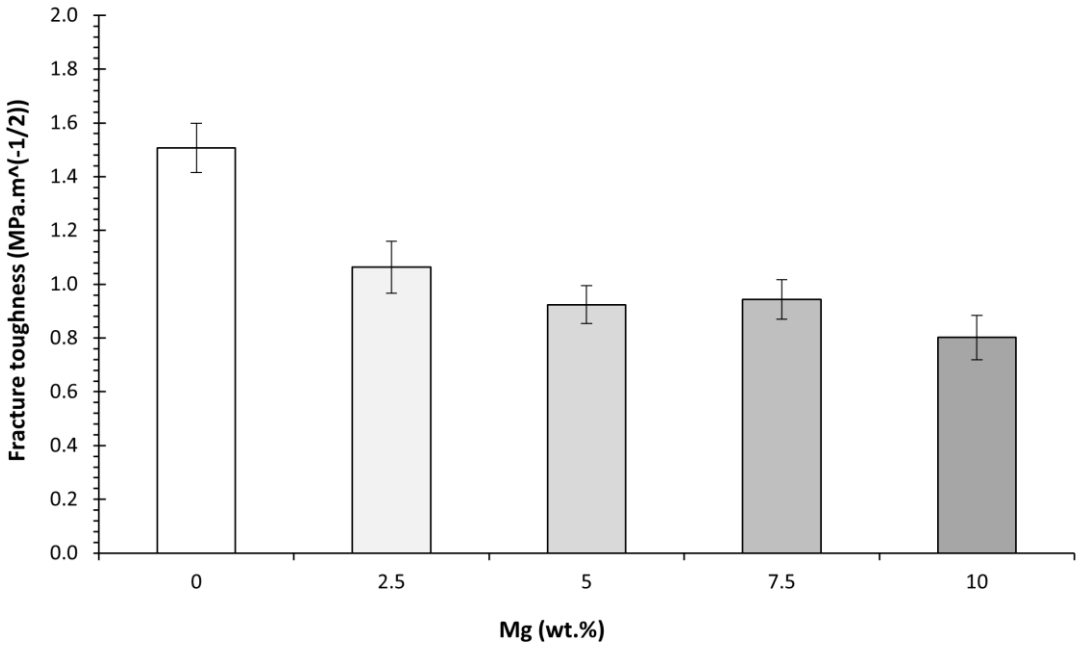

Figure 14 – Evolution of the fracture toughness of PLA-Mg composites with the content of Mg.

It was shown that the tensile strength of PLA also decreases with adding Mg particles. A possible way of understanding this decrease is model 1. In this model 1, it is considered that the porosity decreases the effective area of the PLA cross-section. Previously, it has been observed that the porosity increased with the addition of Mg. Moreover, the PLA-Mg interface was observed to be a weak interface. Thus, the volume occupied by the Mg does not support mechanical loads, and the particles can be assumed as pores for this simplified model 1. All the pores and Mg-like pores have been homogeneously distributed with an infinitesimal diameter size. The theoretical values of the tensile strength for this first model (model 1), are shown in figure 8. A slight decrease of up to 10 % is observed. However, this model does not fit the experimental data. Therefore, the tensile strength reduction must be explained by addressing other effects, like the fracture toughness decrease shown in figure 14.

The theoretical values of the tensile strength for a second model (model 2) are shown in figure 15, in which the fracture toughness of each PLA-Mg composition is considered, together with the increase of the porosity shown in figure 10 and considering the volume of Mg also as porosity. However, this model 2 assumes that the fracture toughness of the PLA matrix has remained constant after processing the PLA-Mg composite. In this scenario, a lower theoretical tensile strength for the PLA-Mg is obtained compared to the experimental one. This is inconsistent with the theory as the decrease of the tensile strength has been underestimated as no consideration of the concentration of stresses around the Mg and pores has been included in the model. This supports the need for a deeper analysis of how the PLA matrix's fracture toughness changes during the PLA-Mg colloidal processing. To compensate the low theoretical values obtained for the tensile strength in this model 2, it is assumed that the fracture toughness of the PLA matrix on the PLA-Mg materials should be higher than the one calculated for the neat PLA (0% Mg). This expected increase in the fracture toughness of the PLA matrix is reasonable considering that the PLA matrix in the PLA-Mg composite has a 5 % weight of PEG, a plasticiser.

Preprints (www.preprints.org) | NOT PEER-REVIEWED | Posted: 5 September 2022 doi:10.20944/preprints202209.0059.v1

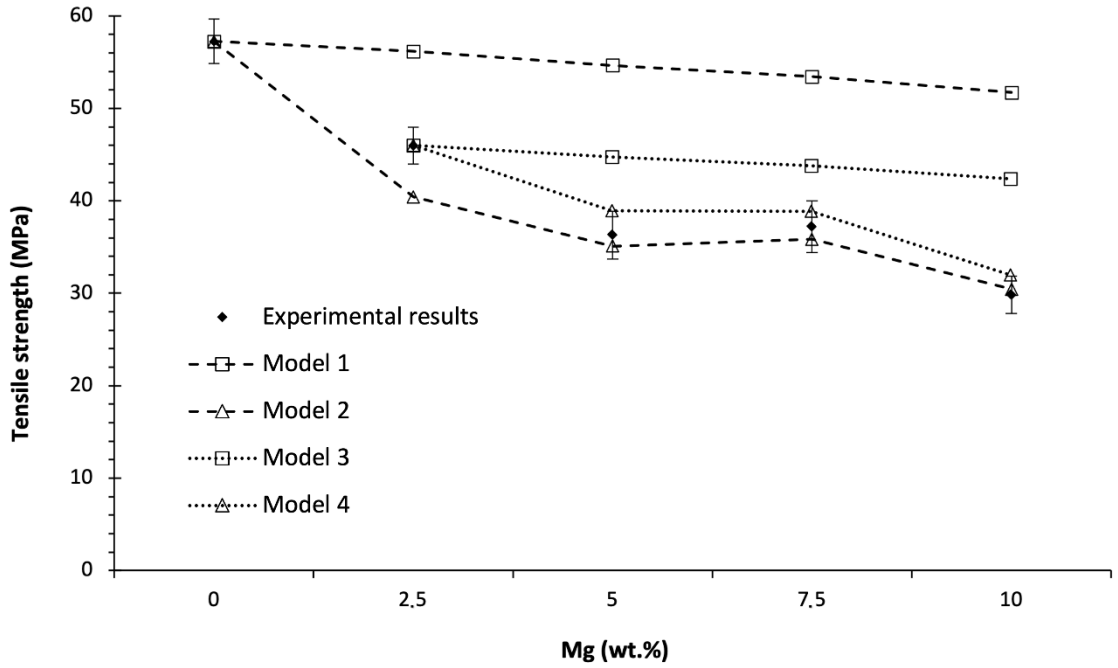

Figure 15 - Evolution of the tensile strength of PLA-Mg composites with the content of Mg particles. Theoretical values of the tensile strength are provided regarding different models. Experimental results are shown in bold.

The third and fourth models (models 3 and 4) were proposed. They are related to models 1 and 2, respectively, using PLA-2.5Mg as the reference material. In these models, it can be assumed that the fracture toughness of the PLA matrix is the same for all the PLA-Mg composites. The results are shown in figure 15. A better fit with the experimental results is obtained, and all the results are higher than the experimental ones, which is more coherent, as these models 3 and 4 do not consider all the possible detrimental effects on the tensile strength. This provides an excellent explanation for understanding the impact of Mg particles on PLA; however, it also indicates that further research is required to assess the influence of the processing on the PLA matrix, as PEG is probably increasing the fracture toughness of the PLA matrix, a common effect of plasticisers on polymers [41]. Last, any impact on the mechanical properties due to differences in the crystallinity at room temperature can be disregarded.

Comparing the literature with the results in this paper, it was found that similar trends have been described for the tensile strength and the DSC, but a direct comparison with this work is hardly possible. Works on PLA and PLA composites usually do not provide information on the ageing times after the materials were prepared [33], [42], a variable that can double the tensile strength (from 30 to 60 MPa) and can take up to 3 months for the PLA to reach the stable mechanical properties at 60 MPa attending to our previous work [20]. However, the norm "Plastics - Determination of tensile properties - Part 1: General principles (ISO 527-1:2019)" indicates a minimum conditioning time of 16 hours before testing, well below the three months required for some commercial PLA studied in the literature.

Without considering if the materials tested in the literature have been entirely aged or not before testing, similar trends for the evolution of PLA-Mg composites can be found [33]. However, the detail of analysis that we present by including the fracture toughness and the modelling of the PLA-Mg composites is not performed in any other work. Moreover, in the literature are found

 doi:10.20944/preprints202209.0059.v1

experiments working on 3D printed samples and no single filaments, which makes it even more challenging to assess the real influence of the Mg particles on the PLA matrix as there are other variables related to the mechanical properties, for example, the adhesion between layers, the printing direction, and the bed temperature, among others. Working directly with the printed filaments decreases the variables that can explain the changes observed in the mechanical properties of the PLA-Mg composites. Regarding DSC results on PLA-Mg composited in the literature, similar DSC graphs are shown in different articles [43], but a deep analysis is not presented.

Combining all the techniques presented here with the study of 1D printed filaments, advances in the knowledge of PLA-Mg composites has been possible.

Further research is required regarding the fracture toughness and the tensile strength decrease of PLA-Mg composites. It is difficult to assess that all the variations of the fracture toughness are solely due to the Mg particles. However, if the samples with Mg content are compared, the **increase of Mg content from 2.5 wt.% to 10 wt.% decreases the fracture toughness and the tensile strength.**

4. Conclusions

This paper contributes to a deeper understanding of the effects of Mg particles (thermal, chemical, physical, and mechanical) on printed PLA-Mg filaments.

The DSC analysis concluded the following aspects:

- PLA-Mg composites have a lower T_g, decreasing with the higher Mg content.
- Mg particles enhance the crystallisation reactions of the α' and α crystals in the PLA.

A hypothesis based on three mechanisms to explain this is proposed: 1) the Mg as a stabiliser of PLA crystals, 2) the addition of PEG (a plasticiser), and 3) the decrease of the molecular weight of the PLA, which is more prominent with the higher content in Mg particles.

The FTIR studies concluded that:

- Chemical interaction between the PLA and the PEI is coherent with the previous work [32] and essential for the mechanical results. However, no interaction between PEG and PLA has been found.
- A slight effect on the bands related to the α crystals is observed; however, almost no crystallinity is kept at room temperature, as expected from the high d-lactide content of the PLA.

Regarding Archimedes' tests, the tensile tests, and the fractography, the conclusions are:

- A Slight increase in the porosity and density due to adding Mg.
- A good dispersion of the Mg particles through the colloidal route is observed in the SEM fractographies.
- A weak PLA-Mg bond, more precisely a weak PEI-Mg bond, explains the elastic modulus evolution by adding Mg. Adding Mg has decreased this weak bond's elastic modulus, tensile strength, and fracture toughness. Note that the weak bond is from a mechanical point of view, as it was strong enough to avoid the formation of Mg agglomerates during the colloidal processing.
- The modelling of the Mg particles as a pore provided a good correlation between theoretical and experimental values for the tensile strength of PLA-Mg composites. However, it also

suggests that the fracture toughness of the PLA matrix in the PLA-Mg composite should be higher than the fracture toughness measured on the neat PLA reference material.

Funding: This research was funded by the Spanish Government (PID2019-106631GB-C44, MICINN/FEDER, UE) and Comunidad de Madrid Government (P2018/NMT-4511 NMAT2D-CM, P2018/NMT-4411 ADITIMAT-CM, FEDER-UE). J. Orellana acknowledges a scholarship provided by UPM and the Ministerio de Educación, Cultura y Deporte of Spain (FPU17/02035).

Institutional Review Board Statement: Not applicable.

Informed Consent Statement: Not applicable.

Conflicts of Interest: The authors declare no conflicts of interest.

References:

[1] M. Fröhlich, W. L. Grayson, L. Q. Wan, D. Marolt, M. Drobnic, and G. Vunjak-Novakovic, "Tissue Engineered Bone Grafts: Biological Requirements, Tissue Culture and Clinical Relevance," *Curr Stem Cell Res Ther*, vol. 3, no. 4, p. 254, Dec. 2008, doi: 10.2174/157488808786733962.

[2] J. Orellana, Y. Y. Pastor, F. Calle, and J. Y. Pastor, "Influence of HRGO Nanoplatelets on Behaviour and Processing of PMMA Bone Cement for Surgery," *Polymers (Basel)*, vol. 13, no. 12, Jun. 2021, doi: 10.3390/POLYM13122027.

[3] H. H. K. Xu *et al.*, "Calcium phosphate cements for bone engineering and their biological properties," *Bone Research 2017 5:1*, vol. 5, no. 1, pp. 1–19, Dec. 2017, doi: 10.1038/boneres.2017.56.

[4] S. Jiang, M. Wang, and J. He, "A review of biomimetic scaffolds for bone regeneration: Toward a cell-free strategy," *Bioengineering & Translational Medicine*, vol. 6, no. 2, May 2021, doi: 10.1002/BTM2.10206.

[5] M. Filippi, G. Born, M. Chaaban, and A. Scherberich, "Natural Polymeric Scaffolds in Bone Regeneration," *Frontiers in Bioengineering and Biotechnology*, vol. 8, p. 474, May 2020, doi: 10.3389/FBIOE.2020.00474/BIBTEX.

[6] X. Bai, M. Gao, S. Syed, J. Zhuang, X. Xu, and X. Q. Zhang, "Bioactive hydrogels for bone regeneration," *Bioactive Materials*, vol. 3, no. 4, pp. 401–417, Dec. 2018, doi: 10.1016/J.BIOACTMAT.2018.05.006.

[7] G. Battafarano *et al.*, "Strategies for Bone Regeneration: From Graft to Tissue Engineering," *Int J Mol Sci*, vol. 22, no. 3, pp. 1–22, Feb. 2021, doi: 10.3390/IJMS22031128.

[8] R. B. Bettman and L. M. Zimmerman, "The use of metal clips in gastrointestinal anastomosis - An experimental study," *American Journal of Digestive Diseases and Nutrition*, vol. 2, no. 5, pp. 318–321, 1935, doi: 10.1007/BF03000817.

[9] H. Zhou, B. Liang, H. Jiang, Z. Deng, and K. Yu, "Magnesium-based biomaterials as emerging agents for bone repair and regeneration: from mechanism to application," *Journal of Magnesium and Alloys*, vol. 9, no. 3, pp. 779–804, May 2021, doi: 10.1016/J.JMA.2021.03.004.

[10] N. Sezer, Z. Evis, S. M. Kayhan, A. Tahmasebifar, and M. Koç, "Review of magnesium-based biomaterials and their applications," *Journal of Magnesium and Alloys*, vol. 6, no. 1, pp. 23–43, Mar. 2018, doi: 10.1016/J.JMA.2018.02.003.

[11] J. M. Seitz, R. Eifler, F. W. Bach, and H. J. Maier, "Magnesium degradation products: Effects on tissue and human metabolism," *Journal of Biomedical Materials Research - Part A*, vol. 102, no. 10, pp. 3744–3753, 2014, doi: 10.1002/JBM.A.35023.

[12] Y. Yang *et al.*, "Mg bone implant: Features, developments and perspectives," *Materials & Design*, vol. 185, p. 108259, Jan. 2020, doi: 10.1016/J.MATDES.2019.108259.

[13] S. Singh, G. Singh, C. Prakash, S. Ramakrishna, L. Lamberti, and C. I. Pruncu, "3D printed biodegradable composites: An insight into mechanical properties of PLA/chitosan scaffold," *Polymer Testing*, vol. 89, p. 106722, Sep. 2020, doi: 10.1016/J.POLYMERTESTING.2020.106722.

[14] T. Distler *et al.*, "Polymer-Bioactive Glass Composite Filaments for 3D Scaffold Manufacturing by Fused Deposition Modeling: Fabrication and Characterisation," *Frontiers in Bioengineering and Biotechnology*, vol. 8, p. 552, Jun. 2020, doi: 10.3389/FBIOE.2020.00552/BIBTEX.

[15] M. Gasparotto *et al.*, "3D Printed Graphene-PLA Scaffolds Promote Cell Alignment and Differentiation," *International Journal of Molecular Sciences 2022, Vol. 23, Page 1736*, vol. 23, no. 3, p. 1736, Feb. 2022, doi: 10.3390/IJMS23031736.

[16] S. L. de Armentia, J. C. del Real, E. Paz, and N. Dunne, "Advances in Biodegradable 3D Printed Scaffolds with Carbon-Based Nanomaterials for Bone Regeneration," *Materials*, vol. 13, no. 22, pp. 1–49, Nov. 2020, doi: 10.3390/MA13225083.

[17] Q. Wang, C. Ji, L. Sun, J. Sun, and J. Liu, "Cellulose Nanofibrils Filled Poly(Lactic Acid) Biocomposite Filament for FDM 3D Printing," *Molecules*, vol. 25, no. 10, May 2020, doi: 10.3390/MOLECULES25102319.

[18] B. Zhang *et al.*, "3D printed bone tissue regenerative PLA/HA scaffolds with comprehensive performance optimisations," *Materials & Design*, vol. 201, p. 109490, Mar. 2021, doi: 10.1016/J.MATDES.2021.109490.

[19] M. Bardot and M. D. Schulz, "Biodegradable Poly(Lactic Acid) Nanocomposites for Fused Deposition Modeling 3D Printing,"

Nanomaterials, vol. 10, no. 12, pp. 1–20, Dec. 2020, doi: 10.3390/NANO10122567.

[20] J. O. Barrasa, A. Ferrández-Montero, B. Ferrari, and J. Y. Pastor, "Characterisation and Modelling of PLA Filaments and Evolution with Time," *Polymers 2021, Vol. 13, Page 2899*, vol. 13, no. 17, p. 2899, Aug. 2021, doi: 10.3390/POLYM13172899.

[21] Y. T. Hsieh, S. Nozaki, M. Kido, K. Kamitani, K. Kojio, and A. Takahara, "Crystal polymorphism of polylactide and its composites by X-ray diffraction study," *Polymer Journal 2020 52:7*, vol. 52, no. 7, pp. 755–763, Apr. 2020, doi: 10.1038/s41428-020-0343-8.

[22] K. Masutani and Y. Kimura, "Synthesis, Structure and Properties of Poly(lactic acid)," *Synthesis, Structure and Properties of Poly(lactic acid)*, vol. 279, pp. 6–7, 2018, doi: 10.1007/978-3-319-64230-7.

[23] R. Auras, B. Harte, and S. Selke, "An overview of polylactides as packaging materials," *Macromol Biosci*, vol. 4, no. 9, pp. 835–864, Sep. 2004, doi: 10.1002/MABI.200400043.

[24] L. T. Sin and B. S. Tueen, "Polylactic acid : a practical guide for the processing, manufacturing, and applications of PLA".

[25] S. A. Khan, S. B. Khan, L. U. Khan, A. Farooq, K. Akhtar, and A. M. Asiri, "Fourier transform infrared spectroscopy: Fundamentals and application in functional groups and nanomaterials characterisation," *Handbook of Materials Characterization*, pp. 317–344, Sep. 2018, doi: 10.1007/978-3-319-92955-2_9.

[26] P. Pan, B. Zhu, W. Kai, T. Dong, and Y. Inoue, "Polymorphic transition in disordered poly(L-lactide) crystals induced by annealing at elevated temperatures," *Macromolecules*, vol. 41, no. 12, pp. 4296–4304, Jun. 2008, doi: 10.1021/MA800343G/ASSET/IMAGES/MEDIUM/MA-2008-00343G_0008.GIF.

[27] L. A. James and W. J. Mills, "Review and synthesis of stress intensity factor solutions applicable to cracks in bolts," *Engineering Fracture Mechanics*, vol. 30, no. 5, pp. 641–654, Jan. 1988, doi: 10.1016/0013-7944(88)90156-7.

[28] D. B. Panemangalore, R. Shabadi, and M. Gupta, "Corrosion behavior, microstructure and mechanical properties of novel mg-zn-ca-er alloy for bio-medical applications," *Metals (Basel)*, vol. 11, no. 3, pp. 1–16, Mar. 2021, doi: 10.3390/MET11030519.

[29] D. Cangialosi, V. M. Boucher, A. Alegría, and J. Colmenero, "Enhanced physical aging of polymer nanocomposites: The key role of the area to volume ratio," *Polymer (Guildf)*, vol. 53, no. 6, pp. 1362–1372, Mar. 2012, doi: 10.1016/J.POLYMER.2012.01.033.

[30] D. J. Hoffman, S. M. Fica-Contreras, and M. D. Fayer, "Amorphous polymer dynamics and free volume element size distributions from

ultrafast IR spectroscopy," *Proc Natl Acad Sci U S A*, vol. 117, no. 25, pp. 13949–13958, Jun. 2020, doi: 10.1073/PNAS.2003225117/SUPPL_FILE/PNAS.2003225117.SAPP.PDF.

[31] S. C. Cifuentes, M. Lieblich, F. A. López, R. Benavente, and J. L. González-Carrasco, "Effect of Mg content on the thermal stability and mechanical behaviour of PLLA/Mg composites processed by hot extrusion," *Mater Sci Eng C Mater Biol Appl*, vol. 72, pp. 18–25, Mar. 2017, doi: 10.1016/J.MSEC.2016.11.037.

[32] A. Ferrández-Montero, M. Lieblich, R. Benavente, J. L. González-Carrasco, and B. Ferrari, "Study of the matrix-filler interface in PLA/Mg composites manufactured by Material Extrusion using a colloidal feedstock," *Additive Manufacturing*, vol. 33, p. 101142, May 2020, doi: 10.1016/j.addma.2020.101142.

[33] C. Pascual-González *et al.*, "Processing and properties of PLA/Mg filaments for 3D printing of scaffolds for biomedical applications," *Rapid Prototyping Journal*, vol. 28, no. 5, pp. 884–894, May 2022, doi: 10.1108/RPJ-06-2021-0152.

[34] H. Xiao, W. Lu, and J. T. Yeh, "Effect of plasticiser on the crystallisation behavior of poly(lactic acid)," *Journal of Applied Polymer Science*, vol. 113, no. 1, pp. 112–121, Jul. 2009, doi: 10.1002/APP.29955.

[35] R. Androsch *et al.*, "Melting of Conformationally Disordered Crystals (α'-Phase) of Poly(l-lactic acid)," *Macromolecular Chemistry and Physics*, vol. 215, no. 11, pp. 1134–1139, Jun. 2014, doi: 10.1002/MACP.201400126.

[36] M. L. di Lorenzo and R. Androsch, "Influence of α'-/α-crystal polymorphism on properties of poly(l-lactic acid)," *Polymer International*, vol. 68, no. 3, pp. 320–334, Mar. 2019, doi: 10.1002/PI.5707.

[37] Y. Kobayashi, T. Ueda, A. Ishigami, and H. Ito, "Changes in Crystal Structure and Accelerated Hydrolytic Degradation of Polylactic Acid in High Humidity," *Polymers (Basel)*, vol. 13, no. 24, Dec. 2021, doi: 10.3390/POLYM13244324.

[38] I. Antoniac, D. Popescu, A. Zapciu, A. Antoniac, F. Miculescu, and H. Moldovan, "Magnesium Filled Polylactic Acid (PLA) Material for Filament Based 3D Printing," *Materials 2019, Vol. 12, Page 719*, vol. 12, no. 5, p. 719, Mar. 2019, doi: 10.3390/MA12050719.

[39] C. A. Rodrigues, A. Tofanello, I. L. Nantes, and D. S. Rosa, "Biological Oxidative Mechanisms for Degradation of Poly(lactic acid) Blended with Thermoplastic Starch," *ACS Sustainable Chemistry and Engineering*, vol. 3, no. 11, pp. 2756–2766, Nov. 2015, doi: 10.1021/ACSSUSCHEMENG.5B00639/SUPPL_FILE/SC5B00639_SI_001.PDF.

 doi:10.20944/preprints202209.0059.v1

[40] B. W. Chieng, N. A. Ibrahim, W. M. Z. W. Yunus, and M. Z. Hussein, "Poly(lactic acid)/poly(ethylene glycol) polymer nanocomposites: Effects of graphene nanoplatelets," *Polymers (Basel)*, vol. 6, no. 1, pp. 93–104, 2014, doi: 10.3390/POLYM6010093.

[41] M. N. Nur Aimi and H. Anuar, "Effect of Plasticiser on Fracture Toughness of Polylactic Acid Reinforced with Kenaf Fibre and Montmorillonite Hybrid Biocomposites," *Engineering Materials*, pp. 263–280, 2016, doi: 10.1007/978-981-10-0950-1_11.

[42] Z. Oksiuta, M. Jalbrzykowski, J. Mystkowska, E. Romanczuk, and T. Osiecki, "Mechanical and thermal properties of polylactide (PLA) composites modified with Mg, Fe, and polyethylene (PE) additives," *Polymers (Basel)*, vol. 12, no. 12, pp. 1–14, Dec. 2020, doi: 10.3390/POLYM12122939.

[43] I. Antoniac, D. Popescu, A. Zapciu, A. Antoniac, F. Miculescu, and H. Moldovan, "Magnesium Filled Polylactic Acid (PLA) Material for Filament Based 3D Printing," *Materials 2019, Vol. 12, Page 719*, vol. 12, no. 5, p. 719, Mar. 2019, doi: 10.3390/MA12050719.